JACS
JOURNAL OF THE AMERICAN CHEMICAL SOCIETY
pubs.acs.org/JACS
Article

In Situ Observation of the pH Gradient near the Gas Diffusion Electrode of CO_2 Reduction in Alkaline Electrolyte

Xu Lu, Chongqin Zhu, Zishan Wu, Jin Xuan, Joseph S. Francisco,* and Hailiang Wang*

Cite This: J. Am. Chem. Soc. 2020, 142, 15438−15444
Read Online

ABSTRACT: The local pH variation near the surface of CO_2 reduction electrodes is important but hard to study. We develop a continuous-flow Raman electrochemical cell that enables the first experimental study of the local pH near a CO_2 reduction gas diffusion electrode under reaction conditions. At zero current, CO_2 chemically reacts with the 1 M KOH electrolyte at the interface to form HCO_3^- and CO_3^{2-}. The local pH on the cathode surface is 7.2, and the HCO_3^- concentration profile extends a distance of 120 μm into the electrolyte, which verifies that the nominal overpotential reduction from using alkaline electrolyte originates from the Nernst potential of the pH gradient layer at the cathode/electrolyte interface. The CO_2−OH^- neutralization reaction and the pH gradient layer still persist, albeit to a reduced extent, at CO_2 reduction current densities up to 150 mA/cm^2.

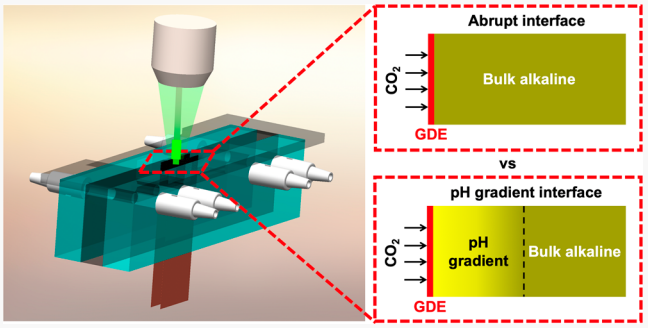

INTRODUCTION

CO_2 electroreduction reactions are promising for producing fuels and chemicals from cheap and abundant CO_2 resources using renewable electricity. Electrochemical conversion of CO_2 to CO,[1−5] formic acid,[6,7] hydrocarbons,[8−11] or alcohols[12−14] allows for the storing of renewable energy in fuels and provides useful chemicals. Conventional three-electrode cells,[15] where the reaction is performed using CO_2 dissolved in the electrolyte, are well-defined for studying electrocatalytic properties of materials. However, the relatively low concentration and sluggish diffusion of CO_2 in the solution phase make it difficult to reach application-relevant high current densities (>0.1 or even 1 A/cm^2). Employing gas diffusion electrodes (GDEs)[16] in flow electrolyzers can greatly enhance the mass transport of CO_2 by forming a gas−liquid−solid three-phase interface and hence substantially increase the diffusion-limited current density.[13,17] While common CO_2 electrolytic cells often use near-neutral aqueous solutions such as $KHCO_3$ as the electrolyte,[18−20] adopting alkaline electrolyte solutions is found to significantly lower the overpotential for CO_2 reduction.[1,3−5,11,14] Current densities greater than 1 A/cm^2 have also been achieved with alkaline electrolytes.[21,22] Despite the improved performance, there is controversy regarding its origin. Some studies attribute this to a simple pH effect assuming the catalyst works in the same alkaline environment as the bulk electrolyte (Figure 1a).[5,22] However, this hypothesis neglects the chemical reaction between CO_2 and OH^- and cannot justify the same magnitude of overpotential reduction experimentally observed for the CO_2-to-CO conversion (two-electron two-proton process) catalyzed by Au and the CO_2-to-formate conversion (two-electron one-proton process) catalyzed by SnO_2 (both ∼60 mV/pH).[1] We therefore postulated that the local environment at the cathode surface is near neutral because of the CO_2−OH^- neutralization reaction (Figure 1b), and the pH gradient across the cathode and the bulk alkaline electrolyte creates a Nernst potential.[1] This can readily explain the voltage improvement observed for all of our alkaline CO_2 electrolyzers using different cathode catalysts for different products and is supported by the observation that the electrolyte is indeed gradually neutralized under continuous working conditions.[1]

To further consolidate this postulation, it is necessary to probe the local pH near the CO_2-reduction GDE in a flow electrolyzer under reaction conditions, which has not been experimentally demonstrated to date. In addition to mathematic models and simulations,[11,23] possible experimental methods to study the local pH include pH-sensitive microelectrodes, rotating disk electrode (RDE) measurements, and spectroscopic tools. Microelectrodes need to be positioned near the catalytic electrode surface and thus inevitably invade the local environment and disrupt the species fluxes there.[24−27] RDE experiments could circumvent this issue and measure the electrode surface pH during hydrogen oxidation/evolution reactions,[28,29] but whether this method would be applicable to

Received: June 24, 2020
Published: July 21, 2020

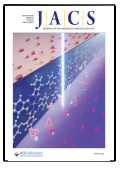

https://dx.doi.org/10.1021/jacs.0c06779
J. Am. Chem. Soc. 2020, 142, 15438−15444

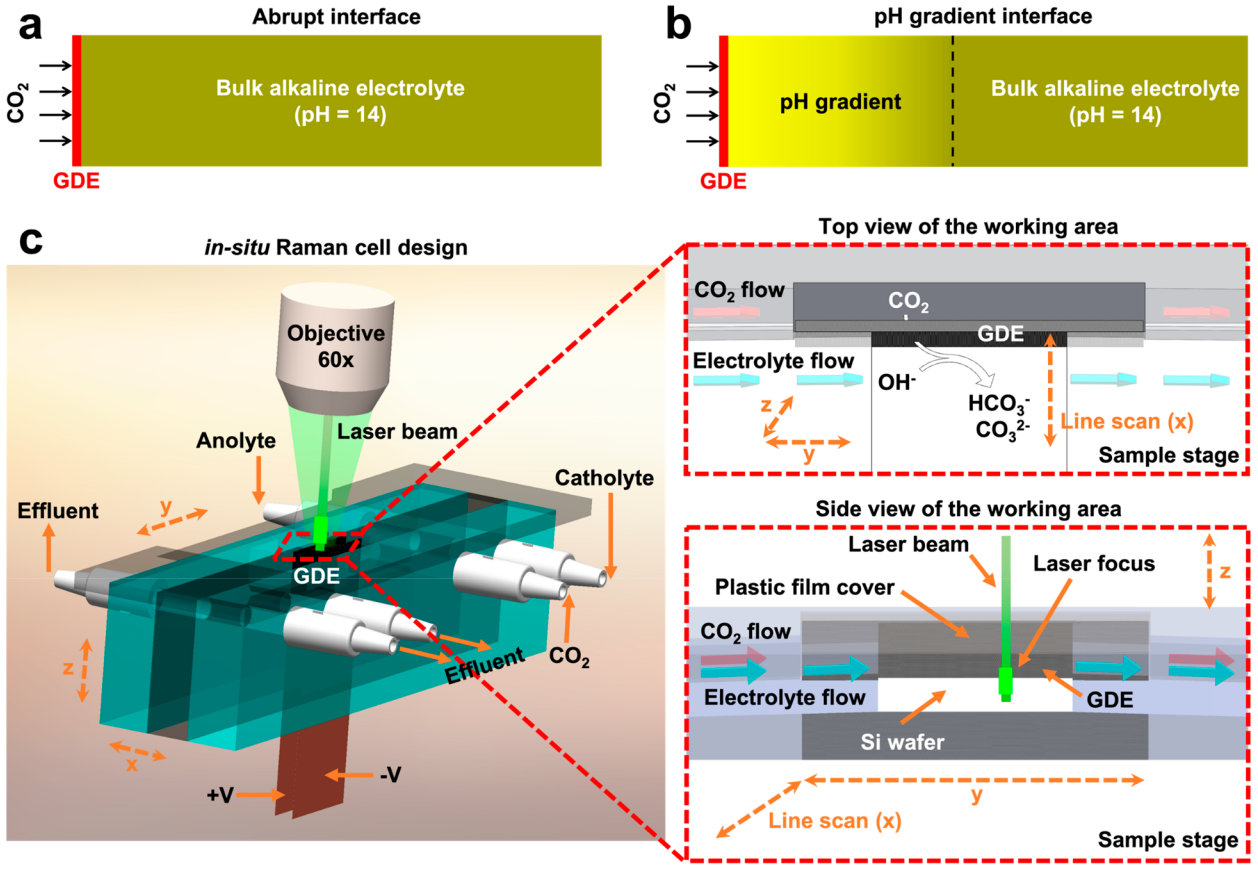

Figure 1. Designed flow cell for performing in situ Raman measurements under continuous-flow CO_2 reduction conditions to distinguish between (a) an abrupt interface and (b) a gradient interface between the cathode and electrolyte. (c) Cell design with top and side views of the cathode area.

CO_2 reduction reactions is not clear. Nondestructive Raman or IR spectroscopy could directly probe pH-sensitive electrolyte species such as carbonate (CO_3^{2-}) and bicarbonate (HCO_3^-) at the electrode/electrolyte interface, but almost all of these studies are conducted on gas-impermeable electrodes, some of which require the catalyst to be coated on a prism and hence are not even compatible with the GDE and flow cell configuration.[30−33]

RESULTS AND DISCUSSION

Herein, we report the design of an alkaline CO_2 electrolyzer that allows in situ Raman microscopy to be performed under continuous flow and reaction conditions to unveil the pH variation from the cathodic GDE surface to the electrolyte bulk. Microarea Raman spectra are recorded to analyze the concentrations of HCO_3^- and CO_3^{2-} as functions of the distance from the electrode surface into the electrolyte bulk, which are extrapolated to the cathode surface assuming steady-state concentrations and acid−base equilibria. The pH values are then derived from the concentrations and equilibrium constants. With 1 M KOH as the electrolyte, we find that under open-circuit conditions the local environment at the cathode surface is near neutral and the pH increases to >11 over a distance of 120 μm into the electrolyte, which is attributed to the CO_2−OH^- neutralization reaction. Applying a reduction current raises the pH near the cathode surface and narrows the pH gradient layer, largely due to the generation of OH^- from the electrochemical CO_2 reduction reaction. However, the generated OH^- at current densities up to 150 mA/cm^2 can still not balance the consumption from the chemical reaction with CO_2. These results confirm that the overpotential reduction of alkaline CO_2 electrolyzers as compared to neutral ones originates from the pH gradient at the cathode/electrolyte interface.

We modified our previously developed flow electrolyzer[1,18] to allow for examination using a confocal Raman microscope under reaction conditions (Figure 1c). In this configuration, the micrometer-size laser beam is parallel to the GDE surface, which separates the CO_2 gas and liquid electrolyte. The distance from the laser beam to the electrode surface is controlled by the mechanical sample stage for line scan measurements (Figure 1c, top view). We chose HCO_3^- and CO_3^{2-} as pH probes because (i) they are the products of the CO_2−OH^- neutralization reaction, which avoids any interference from incorporating additional pH-sensitive species, (ii) they have distinguishable Raman features and can be independently quantified using calibration curves (Figure S1), and (iii) the acid−base equilibrium between them can be used to derive the pH.

We first studied the system at open circuit with 1 M KOH electrolyte flowing at 0.5 mL/min and CO_2 flowing at 20 sccm. This zero-current scenario corresponds to situations when the cathode potential is more positive than the onset potential for CO_2 reduction. As shown in Figure 2a, HCO_3^- and CO_3^{2-} peaks are recorded at 1012 and 1064 cm^{-1}, respectively, when the laser beam is positioned 10 μm away from the cathode into the electrolyte (x = −10 μm, where x denotes the distance from the cathode surface and the negative sign indicates the

https://dx.doi.org/10.1021/jacs.0c06779
J. Am. Chem. Soc. 2020, 142, 15438−15444

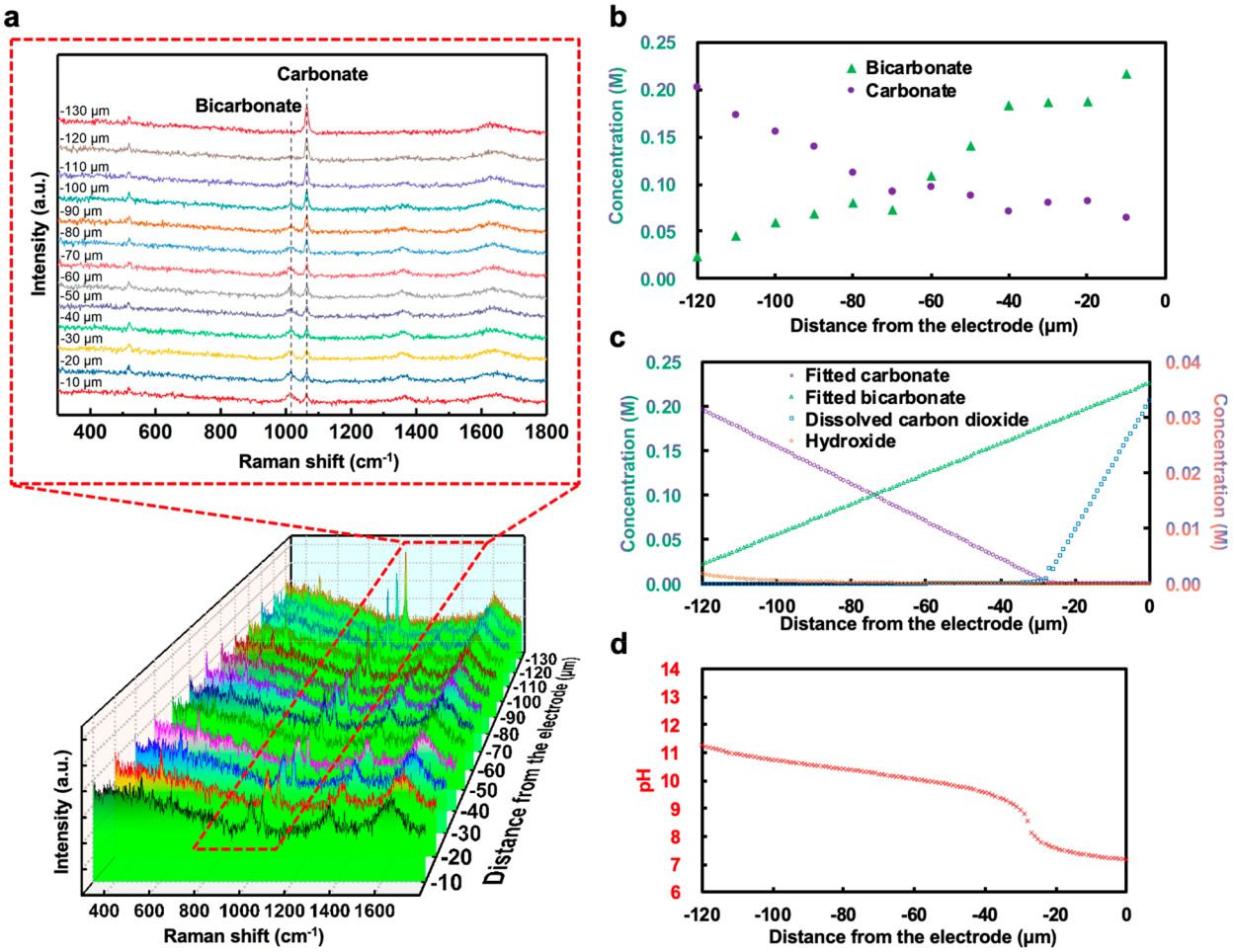

Figure 2. (a) Raman spectra recorded at various distances from the GDE surface. Current density: 0 mA/cm^2. Electrolyte: 1 M KOH. (b) HCO_3^- and CO_3^{2-} concentrations derived from the spectra in (a). (c) Fitted concentrations of HCO_3^-, CO_3^{2-}, CO_2 (aq), and OH^- and (d) pH profile with respect to the distance from the GDE surface.

direction from the cathode to the electrolyte). The existence of HCO_3^- and CO_3^{2-} unambiguously proves that CO_2 reacts with the alkaline electrolyte, at least when there is no net CO_2 electroreduction. As the laser beam is moved further away from the GDE surface into the electrolyte, the detected HCO_3^- concentration decreased from 0.22 M at $x = -10$ μm to 0.024 M at $x = -120$ μm, and the CO_3^{2-} concentration increased from 0.065 to 0.20 M (Figure 2b). These trends indicate that the HCO_3^- originates from the CO_2–OH^- neutralization at the cathode/electrolyte interface and diffuses into the KOH electrolyte where it is further deprotonated to form CO_3^{2-}.

Note that the trends of concentration change for both HCO_3^- and CO_3^{2-} are less well-defined in the region of -40 μm $< x < 0$ μm (Figure 2b). We believe this is due to the poor spatial resolution of our Raman measurements in this region, which is much worse than the optimal micrometer level because (i) the laser beam is focused into liquid instead of on a substrate, (ii) the electrolyte is flowing, and (iii) there is likely interference from the nearby electrode. Therefore, the HCO_3^- and CO_3^{2-} concentrations directly derived from the Raman spectra need to be corrected. We consider that in our system the region of interest can be treated as a quasi-one-dimensional channel (Figure 1b). The concentrations of the species of interest are dependent on x but are uniform along the y and z directions.[28,34] The concentration of HCO_3^- at any given position x is influenced by both acid–base reactions and diffusion:

$$\frac{\partial c_1}{\partial t} = D_1\frac{\partial^2 c_1}{\partial x^2} + k_{1f}c_3c_4 - k_{1r}c_1 - k_{2f}c_1c_3 + k_{2r}c_2 \quad (1)$$

where c_1, c_2, c_3, and c_4 are the concentrations of HCO_3^-, CO_3^{2-}, OH^-, and CO_2(aq), respectively, D_1 is the diffusion coefficient of HCO_3^-, and k_{1f}, k_{1r}, k_{2f}, and k_{2r} are the forward and reverse reaction rate constants of the following two reactions:

$$CO_2(aq) + OH^- \rightleftharpoons HCO_3^- \quad (I)$$

$$HCO_3^- + OH^- \rightleftharpoons CO_3^{2-} + H_2O \quad (II)$$

We assume reactions I and II are at equilibrium, which means $k_{1f}c_3c_4 = k_{1r}c_1$ and $k_{2f}c_1c_3 = k_{2r}c_2$. In the steady state, the concentration of HCO_3^- does not change over time, that is, $\frac{\partial c_1}{\partial t} = 0$. Equation 1 can therefore be simplified to $\frac{\partial^2 c_1}{\partial x^2} = 0$, which suggests the concentration of HCO_3^- should be linear with respect to x. The same analysis applies to CO_3^{2-} and CO_2(aq). Therefore, we used the HCO_3^- and CO_3^{2-} concentration data measured in the region of -120 μm $\leq x \leq -40$ μm to fit linear functions of x, because in this region they are reasonably linear with respect to x and the detection is

https://dx.doi.org/10.1021/jacs.0c06779
J. Am. Chem. Soc. 2020, 142, 15438−15444

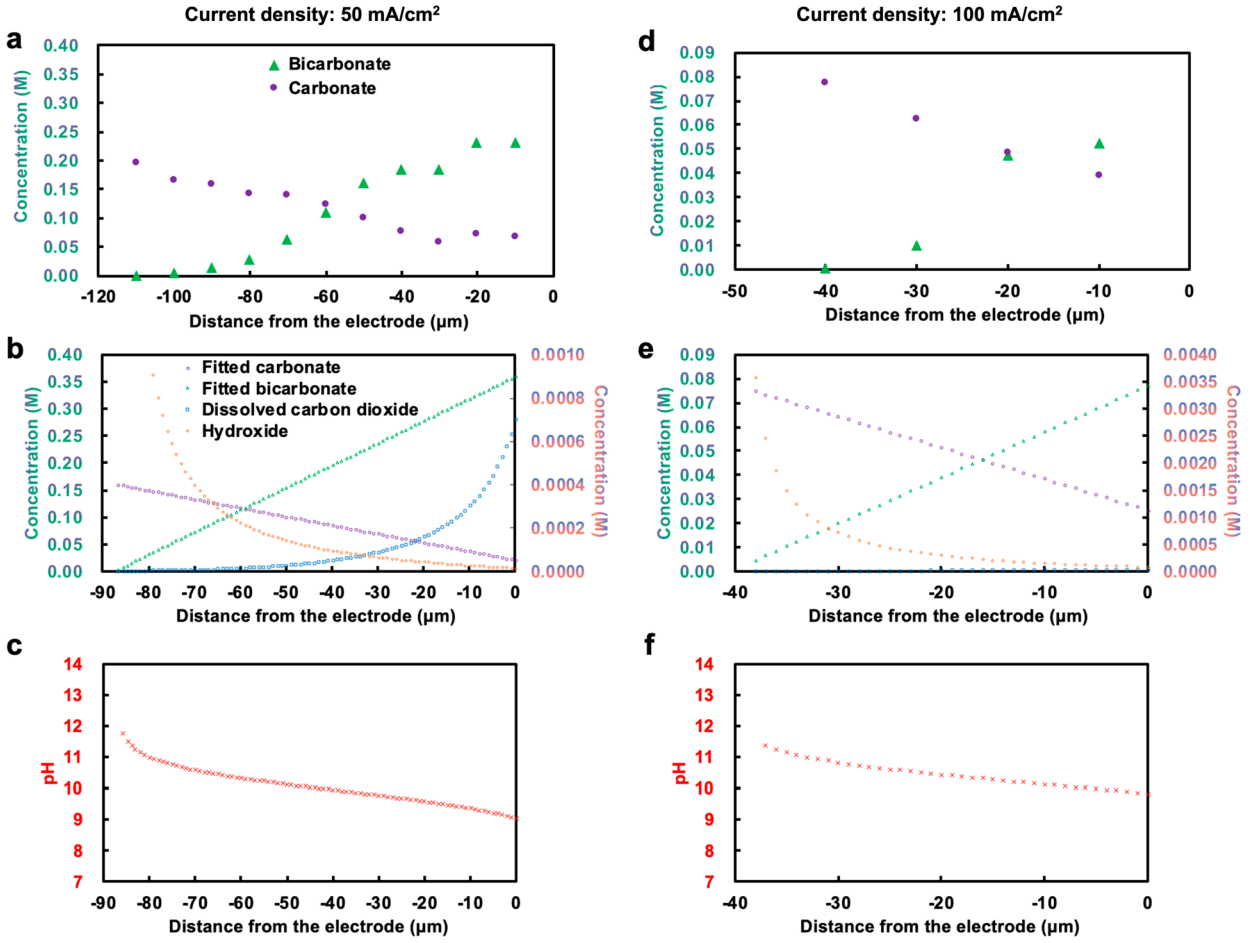

Figure 3. Measured HCO_3^- and CO_3^{2-} concentrations with respect to the distance from the GDE surface at current densities of (a) 50 mA/cm^2 and (d) 100 mA/cm^2. Electrolyte: 1 M KOH. (b and e) Fitted concentrations of HCO_3^-, CO_3^{2-}, CO_2 (aq), and OH^- corresponding to (a) and (d), respectively. (c and f) pH profiles derived from (b) and (e), respectively.

not disrupted by the electrode. As shown in Figure 2c, in the region from $x = -120$ μm to $x = -26$ μm, HCO_3^- and CO_3^{2-} are dominant species, and the HCO_3^- concentration increases linearly with x from 0.022 to 0.18 M, while the CO_3^{2-} concentration decreases linearly with x from 0.20 to 0.0012 M. In the region of -26 μm $\leq x \leq 0$ μm, the concentration of CO_3^{2-} approaches zero, and the dominant species are HCO_3^- and CO_2(aq). The HCO_3^- concentration increases from 0.18 M at $x = -26$ μm to 0.23 M at $x = 0$ μm, and the CO_2(aq) concentration increases from 0.0028 M at $x = -26$ μm to its saturated level at $x = 0$ μm, that is, 0.033 M.[35] As minor species, the concentrations of CO_2(aq) in the -120 μm $\leq x \leq -26$ μm region, CO_3^{2-} in the -26 μm $\leq x \leq 0$ μm region, and OH^- in the entire region can be calculated from the acid–base equilibria (Figure 2c). More detailed analysis and fitting results are available in the Supporting Information. As shown in Figure 2d, the pH profile for the pH gradient region can be divided into two regimes, one governed by the CO_2/HCO_3^- buffer pair and the other by HCO_3^-/CO_3^{2-}. At $x = 0$ μm, that is, the cathode/electrolyte interface, the pH is 7.2, which suggests that the KOH electrolyte is almost completely neutralized by CO_2. The pH increases to >11 at $x = -120$ μm and starts to approach that of the bulk electrolyte.

The foundation of our analysis is the assumption of acid–base equilibrium, which we made on the basis that the two neutralization reactions, that is, reactions I and II, are fast with $k_{1f} = 5.93 \times 10^3$ M^{-1} s^{-1} and $k_{2f} = 1 \times 10^8$ M^{-1} s^{-1}. To further confirm the validity of this assumption, we carried out two sets of experiments. We noticed that the total concentration of negative charges from HCO_3^- and CO_3^{2-} in the scanned region is approximately 0.4 M (Figure S2), which is significantly below the concentration of the starting 1 M KOH electrolyte. This raised a concern whether there is still a high concentration of OH^- in this region. If so, reactions I and II are not at equilibrium, which would violate our assumption. To examine this issue, we replaced the 1 M KOH electrolyte with a $N(CH_3)_4OH$ electrolyte of the same concentration so that the cation concentration can be quantified by Raman spectroscopy (Figures S3 and S4). Under identical operating conditions, the $N(CH_3)_4^+$ concentration over -110 μm $\leq x \leq -10$ μm is found to be approximately 0.4 M (Figure S5), in good agreement with the total charge concentration of HCO_3^- and CO_3^{2-}. Because charge neutrality always prevails, this result suggests that OH^- is indeed a minor species in the pH gradient region and the acid–base equilibria hold. The electrolyte concentration in this region is significantly lower than that of the bulk because OH^- is almost fully consumed by CO_2 and the formed HCO_3^- and CO_3^{2-} diffuse. As evidence, we found that the $N(CH_3)_4^+$ concentration is around 1 M when CO_2 is replaced with Ar (Figure S6). In another experiment, we varied the flow rates of CO_2 and KOH electrolyte independently. We first changed the CO_2 gas flow

https://dx.doi.org/10.1021/jacs.0c06779
J. Am. Chem. Soc. 2020, 142, 15438–15444

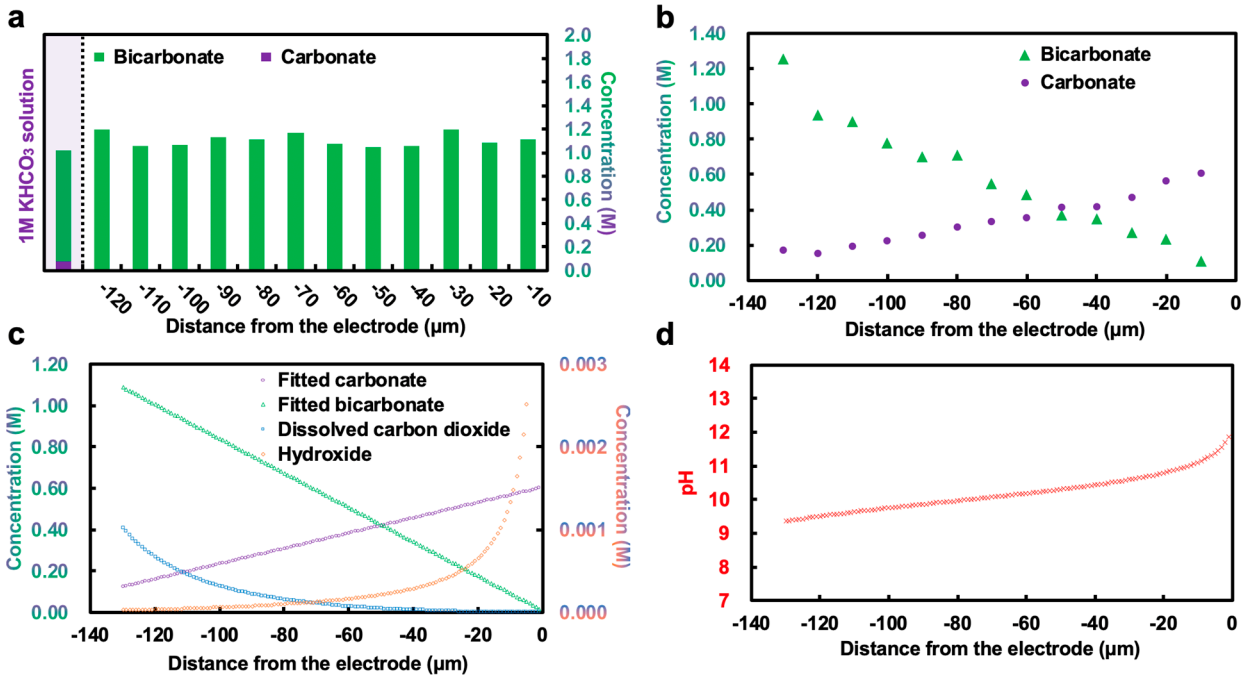

Figure 4. Measured HCO_3^- and CO_3^{2-} concentrations with respect to the distance from the GDE surface at current densities of (a) 0 mA/cm^2 and (b) 50 mA/cm^2. Electrolyte: 1 M $KHCO_3$. (c) Fitted concentrations of HCO_3^-, CO_3^{2-}, CO_2 (aq), and OH^- and (d) pH profile with respect to the distance from the GDE surface.

rate between 5 and 25 sccm at a fixed electrolyte flow rate of 0.5 mL/min. The result shows that at higher gas flow rates, more CO_2 reacts with the electrolyte and the pH gradient region is wider. At 5 sccm, HCO_3^- is detectable until $x = -70$ μm; when the CO_2 flow rate is increased to 25 sccm, HCO_3^- penetrates to $x = -130$ μm (Figure S7). We also changed the electrolyte flow rate between 0.6 and 0.1 mL/min at a fixed CO_2 flow rate of 20 sccm. The pH gradient region becomes wider at slower electrolyte flow rates (Figure S8). The responses of the HCO_3^- and CO_3^{2-} concentration profiles to the gas and electrolyte flow rates again verify that our system is not limited by the kinetics of the acid–base reactions.

We then operated the electrochemical cell at constant-current CO_2 reduction conditions and performed in situ Raman measurements to study the pH changes near the GDE surface. In the current density range studied, the catalyst, cobalt phthalocyanine molecules supported on carbon nanotubes (CoPc/CNT), converts CO_2 to CO with high selectivity (Figure S9).[1,2] The conversion of CO_2 to CO consumes protons likely from H_2O and thus generates OH^-, which can counter the effect of CO_2–OH^- neutralization on the local pH. At the current density of 50 mA/cm^2 (Figure S10), the HCO_3^- concentration near the cathode surface ($x = -10$ μm) is measured to be 0.23 M, which decreases to 0.029 M at $x = -80$ μm, and the CO_3^{2-} concentration increases from 0.07 M at $x = -10$ μm to 0.14 M at $x = -80$ μm (Figures 3a and S11). The region where HCO_3^- is detectable is 40 μm narrower at 50 mA/cm^2 than that in the open-circuit scenario (Figure 2b). Fitting the experimentally measured HCO_3^- and CO_3^{2-} concentrations as linear functions of x gives smooth concentration profiles (Figure 3b), from which the pH profile can be derived. As shown in Figure 3c, the local pH at the electrode/electrolyte interface is 9.05, much higher than that in the open-circuit scenario (Figure 2d), and the HCO_3^- region is about 86 μm. When the current density is increased to 100 mA/cm^2 (Figure S12), the HCO_3^- region further shrinks to 37 μm (Figures 3d,e and S13), and the cathode surface pH is determined to be 9.8 (Figure 3f). When the current density reaches 150 mA/cm^2 (Figure S14), only CO_3^{2-} can be observed at $x = -10$ μm (Figure S15), which indicates a cathode surface pH higher than 12. These findings confirm that the electrochemical CO_2 reduction reaction indeed produces OH^- at the cathode surface;[1,5] however, the produced OH^- cannot fully offset the OH^- consumed by the chemical reaction with CO_2 even at a high current density of 150 mA/cm^2. In fact, as long as the one-pass CO_2 conversion is not 100%, the unreacted CO_2 will react with KOH at the interface.

The acid–base reaction between CO_2 and electrolyte occurs even when a 1 M $KHCO_3$ aqueous solution is used as the electrolyte. As shown in Figure 4a, both HCO_3^- and CO_3^{2-} are detected by Raman spectroscopy in the bulk of the 1 M $KHCO_3$ electrolyte (purple highlight), whereas no CO_3^{2-} signal is found near the cathode surface in the region of -120 μm $\leq x \leq -10$ μm. This is strong evidence that the CO_2 gas reacts with the CO_3^{2-} in the electrolyte to form HCO_3^-. When the electrochemical CO_2 reduction reaction proceeds at 50 mA/cm^2 (Figure S16), both HCO_3^- and CO_3^{2-} are present in the region of -130 μm $\leq x \leq -10$ μm. The CO_3^{2-} concentration drops from 0.61 M at $x = -10$ μm to 0.18 M at $x = -130$ μm, while the HCO_3^- concentration increases from 0.11 M at $x = -10$ μm to 1.26 M at $x = -130$ μm (Figure 4b). Fitting these measured concentrations into linear functions of x gives concentration and pH profiles (Figure 4c,d), which show that the local pH near the cathode surface is 11.9, much higher than that of the electrolyte bulk. Note that under these conditions, CO_2 will still chemically react with the electrolyte, and the reaction rate would be even faster than that in the zero-current scenario because the local pH is now higher. However, the CO_2-electrolyte neutralization reaction is not

https://dx.doi.org/10.1021/jacs.0c06779
J. Am. Chem. Soc. 2020, 142, 15438–15444

significant enough to balance the OH^- generated from the electrochemical CO_2 reduction reaction, which is the driving force of the basic local pH.

CONCLUSION

We have demonstrated that in situ microarea Raman spectroscopy is an effective tool for studying the local pH near CO_2 reduction GDEs under working conditions. Applying this technique, we have obtained experimental evidence that CO_2 chemically reacts with alkaline electrolyte at the interface. This neutralization reaction has significant influences on the local pH and the electrochemical performance. This continuous-flow Raman electrochemical cell could also be applicable to other reaction systems involving GDEs. The spatial resolution and Raman sensitivity might be limitations, which could be overcome by techniques such as surface enhancement.

ASSOCIATED CONTENT

Supporting Information

The Supporting Information is available free of charge at https://pubs.acs.org/doi/10.1021/jacs.0c06779.

Experimental details, concentration profile fitting, and supplementary figures (PDF)

AUTHOR INFORMATION

Corresponding Authors

Joseph S. Francisco − *Department of Earth and Environmental Science and Department of Chemistry, University of Pennsylvania, Philadelphia, Pennsylvania 19104, United States;* orcid.org/0000-0002-5461-1486; Email: frjoseph@sas.upenn.edu

Hailiang Wang − *Department of Chemistry and Energy Sciences Institute, Yale University, New Haven, Connecticut 06520, United States;* orcid.org/0000-0003-4409-2034; Email: hailiang.wang@yale.edu

Authors

Xu Lu − *Department of Chemistry and Energy Sciences Institute, Yale University, New Haven, Connecticut 06520, United States*

Chongqin Zhu − *Department of Earth and Environmental Science and Department of Chemistry, University of Pennsylvania, Philadelphia, Pennsylvania 19104, United States*

Zishan Wu − *Department of Chemistry and Energy Sciences Institute, Yale University, New Haven, Connecticut 06520, United States;* orcid.org/0000-0003-4810-9112

Jin Xuan − *Department of Chemical Engineering, Loughborough University, Loughborough LE11 3TU, United Kingdom;* orcid.org/0000-0002-6718-9018

Complete contact information is available at: https://pubs.acs.org/10.1021/jacs.0c06779

Notes

The authors declare no competing financial interest.

ACKNOWLEDGMENTS

This work was supported by the National Science Foundation (Grant CHE-1651717). X.L. acknowledges the Croucher Fellowship for Postdoctoral Research. J.S.F. acknowledges support from the National Science Foundation (Grant CHE-1665324). H.W. acknowledges support from the Sloan Research Fellowship. We thank Dr. Yifei Wang (Department of Mechanical Engineering, University of Hong Kong) for assistance with cell fabrication.

REFERENCES

(1) Lu, X.; Wu, Y.; Yuan, X.; Huang, L.; Wu, Z.; Xuan, J.; Wang, Y.; Wang, H. High-performance electrochemical CO_2 reduction cells based on non-noble metal catalysts. *ACS Energy Letters* **2018**, *3* (10), 2527−2532.

(2) Zhang, X.; Wu, Z.; Zhang, X.; Li, L.; Li, Y.; Xu, H.; Li, X.; Yu, X.; Zhang, Z.; Liang, Y.; Wang, H. Highly selective and active CO_2 reduction electrocatalysts based on cobalt phthalocyanine/carbon nanotube hybrid structures. *Nat. Commun.* **2017**, *8*, 14675.

(3) Wang, M.; Torbensen, K.; Salvatore, D.; Ren, S.; Joulié, D.; Dumoulin, F.; Mendoza, D.; Lassalle Kaiser, B.; Işci, U.; Berlinguette, C. P.; Robert, M. CO_2 electrochemical catalytic reduction with a highly active cobalt phthalocyanine. *Nat. Commun.* **2019**, *10*, 3602.

(4) Salvatore, D. A.; Weekes, D. M.; He, J.; Dettelbach, K. E.; Li, Y. C.; Mallouk, T. E.; Berlinguette, C. P. Electrolysis of gaseous CO_2 to CO in a flow cell with a bipolar membrane. *ACS Energy Letters* **2018**, *3* (1), 149−154.

(5) Verma, S.; Hamasaki, Y.; Kim, C.; Huang, W.; Lu, S.; Jhong, H. R. M.; Gewirth, A. A.; Fujigaya, T.; Nakashima, N.; Kenis, P. J. Insights into the low overpotential electroreduction of CO_2 to CO on a supported gold catalyst in an alkaline flow electrolyzer. *ACS Energy Letters* **2018**, *3* (1), 193−198.

(6) Lu, X.; Wu, Y.; Yuan, X.; Wang, H. An integrated CO_2 electrolyzer and formate fuel cell enabled by a reversibly restructuring Pb-Pd bimetallic catalyst. *Angew. Chem., Int. Ed.* **2019**, *58* (12), 4031−4035.

(7) Gao, D.; Zhou, H.; Cai, F.; Wang, D.; Hu, Y.; Jiang, B.; Cai, W. B.; Chen, X.; Si, R.; Yang, F.; Miao, S.; Wang, J.; Wang, G.; Bao, X. Switchable CO_2 electroreduction via engineering active phases of Pd nanoparticles. *Nano Res.* **2017**, *10*, 2181−2191.

(8) Zheng, Y.; Vasileff, A.; Zhou, X.; Jiao, Y.; Jaroniec, M.; Qiao, S. Z. Understanding the roadmap for electrochemical reduction of CO_2 to multi-carbon oxygenates and hydrocarbons on copper-based catalysts. *J. Am. Chem. Soc.* **2019**, *141* (19), 7646−7659.

(9) Ma, M.; Djanashvili, K.; Smith, W. A. Controllable hydrocarbon formation from the electrochemical reduction of CO_2 over Cu nanowire arrays. *Angew. Chem., Int. Ed.* **2016**, *55* (23), 6680−6684.

(10) Weng, Z.; Wu, Y.; Wang, M.; Jiang, J.; Yang, K.; Huo, S.; Wang, X. F.; Ma, Q.; Brudvig, G. W.; Batista, V. S.; Liang, Y.; Feng, Z.; Wang, H. Active sites of copper-complex catalytic materials for electrochemical carbon dioxide reduction. *Nat. Commun.* **2018**, *9*, 415.

(11) Dinh, C. T.; Burdyny, T.; Kibria, M. G.; Seifitokaldani, A.; Gabardo, C. M.; de Arquer, F. P. G.; Kiani, A.; Edwards, J. P.; De Luna, P.; Bushuyev, O. S.; Zhou, C.; Quintero-Bermudez, R.; Pang, Y.; Sinton, D.; Sargent, E. H. CO_2 electroreduction to ethylene via hydroxide-mediated copper catalysis at an abrupt interface. *Science* **2018**, *360* (6390), 783−787.

(12) Wu, Y.; Jiang, Z.; Lu, X.; Liang, Y.; Wang, H. Domino electroreduction of CO_2 to methanol on a molecular catalyst. *Nature* **2019**, *575*, 639−642.

(13) Li, F.; Li, Y. C.; Wang, Z.; Li, J.; Nam, D. H.; Lum, Y.; Luo, M.; Wang, X.; Ozden, A.; Hung, S. F.; Chen, B.; Wang, Y.; Wicks, J.; Xu, Y.; Li, Y.; Gabardo, C. M.; Dinh, C. T.; Wang, Y.; Zhuang, T. T.; Sinton, D.; Sargent, E. H. Cooperative CO_2-to-ethanol conversion via enriched intermediates at molecule-metal catalyst interfaces. *Nature Catalysis* **2020**, *3*, 75−82.

(14) Lv, J. J.; Jouny, M.; Luc, W.; Zhu, W.; Zhu, J. J.; Jiao, F. A highly porous copper electrocatalyst for carbon dioxide reduction. *Adv. Mater.* **2018**, *30* (49), 1803111.

(15) Clark, E. L.; Resasco, J.; Landers, A.; Lin, J.; Chung, L. T.; Walton, A.; Hahn, C.; Jaramillo, T. F.; Bell, A. T. Standards and protocols for data acquisition and reporting for studies of the electrochemical reduction of carbon dioxide. *ACS Catal.* **2018**, *8* (7), 6560−6570.

(16) Cindrella, L.; Kannan, A. M.; Lin, J.; Saminathan, K.; Ho, Y.; Lin, C.; Wertz, J. Gas diffusion layer for proton exchange membrane fuel cells - A review. *J. Power Sources* **2009**, *194* (1), 146−160.
(17) Liu, K.; Smith, W. A.; Burdyny, T. Introductory guide to assembling and operating gas diffusion electrodes for electrochemical CO_2 reduction. *ACS Energy Letters* **2019**, *4* (3), 639−643.
(18) Lu, X.; Jiang, Z.; Yuan, X.; Wu, Y.; Malpass Evans, R.; Zhong, Y.; Liang, Y.; McKeown, N. B.; Wang, H. A bio-inspired O_2-tolerant catalytic CO_2 reduction electrode. *Science Bulletin* **2019**, *64* (24), 1890−1895.
(19) Gu, J.; Hsu, C.-S.; Bai, L.; Chen, H. M.; Hu, X. Atomically dispersed Fe^{3+} sites catalyze efficient CO_2 electroreduction to CO. *Science* **2019**, *364* (6445), 1091−1094.
(20) Loiudice, A.; Lobaccaro, P.; Kamali, E. A.; Thao, T.; Huang, B. H.; Ager, J. W.; Buonsanti, R. Tailoring copper nanocrystals towards C2 products in electrochemical CO_2 reduction. *Angew. Chem., Int. Ed.* **2016**, *55* (19), 5789−5792.
(21) de Arquer, F. P. G.; Dinh, C. T.; Ozden, A.; Wicks, J.; McCallum, C.; Kirmani, A. R.; Nam, D. H.; Gabardo, C.; Seifitokaldani, A.; Wang, X.; Li, Y. C.; Li, F.; Edwards, J.; Richter, L. J.; Thorpe, S. J.; Sinton, D.; Sargent, E. H. CO_2 electrolysis to multicarbon products at activities greater than 1 A cm^{-2}. *Science* **2020**, *367* (6478), 661−666.
(22) Ma, W.; Xie, S.; Liu, T.; Fan, Q.; Ye, J.; Sun, F.; Jiang, Z.; Zhang, Q.; Cheng, J.; Wang, Y. Electrocatalytic reduction of CO_2 to ethylene and ethanol through hydrogen-assisted C-C coupling over fluorine-modified copper. *Nature Catalysis* **2020**, *3*, 478−487.
(23) Gupta, N.; Gattrell, M.; MacDougall, B. Calculation for the cathode surface concentrations in the electrochemical reduction of CO_2 in $KHCO_3$ solutions. *J. Appl. Electrochem.* **2006**, *36*, 161−172.
(24) Honda, T.; Murase, K.; Hirato, T.; Awakura, Y. pH measurement in the vicinity of a cathode evolving hydrogen gas using an antimony microelectrode. *J. Appl. Electrochem.* **1998**, *28*, 617−622.
(25) Wolfe, R. C.; Weil, K. G.; Shaw, B. A.; Pickering, H. W. Measurement of pH gradients in the crevice corrosion of iron using a palladium hydride microelectrode. *J. Electrochem. Soc.* **2005**, *152* (2), B82−B88.
(26) Morris, C. A.; Chen, C. C.; Ito, T.; Baker, L. A. Local pH measurement with scanning ion conductance microscopy. *J. Electrochem. Soc.* **2013**, *160* (8), H430−H435.
(27) Henstridge, M. C.; Wildgoose, G. G.; Compton, R. G. Generator-collector experiments at a single electrode: Exploring the general applicability of this approach by comparing the performance of surface immobilized versus solution phase sensing molecules. *Langmuir* **2010**, *26* (2), 1340−1346.
(28) Auinger, M.; Katsounaros, I.; Meier, J. C.; Klemm, S. O.; Biedermann, P. U.; Topalov, A. A.; Rohwerder, M.; Mayrhofer, K. J. Near-surface ion distribution and buffer effects during electrochemical reactions. *Phys. Chem. Chem. Phys.* **2011**, *13*, 16384−16394.
(29) Katsounaros, I.; Meier, J. C.; Klemm, S. O.; Topalov, A. A.; Biedermann, P. U.; Auinger, M.; Mayrhofer, K. J. The effective surface pH during reactions at the solid-liquid interface. *Electrochem. Commun.* **2011**, *13* (6), 634−637.
(30) Cannan, S.; Macklam, I. D.; Unwin, P. R. Three-dimensional imaging of proton gradients at microelectrode surfaces using confocal laser scanning microscopy. *Electrochem. Commun.* **2002**, *4* (11), 886−892.
(31) Rudd, N. C.; Cannan, S.; Bitziou, E.; Ciani, I.; Whitworth, A. L.; Unwin, P. R. Fluorescence confocal laser scanning microscopy as a probe of pH gradients in electrode reactions and surface activity. *Anal. Chem.* **2005**, *77* (19), 6205−6217.
(32) Jiang, S.; Klingan, K.; Pasquini, C.; Dau, H. New aspects of operando Raman spectroscopy applied to electrochemical CO_2 reduction on Cu foams. *J. Chem. Phys.* **2019**, *150*, 041718.
(33) Yang, K.; Kas, R.; Smith, W. A. In situ infrared spectroscopy reveals persistent alkalinity near electrode surfaces during CO_2 electroreduction. *J. Am. Chem. Soc.* **2019**, *141* (40), 15891−15900.
(34) Carneiro Neto, E. B.; Lopes, M. C.; Pereira, E. C. Simulation of interfacial pH changes during hydrogen evolution reaction. *J. Electroanal. Chem.* **2016**, *765*, 92−99.
(35) Li, T.; Lees, E. W.; Goldman, M.; Salvatore, D. A.; Weekes, D. M.; Berlinguette, C. P. Electrolytic conversion of bicarbonate into CO in a flow cell. *Joule* **2019**, *3* (6), 1487−1497.

https://dx.doi.org/10.1021/jacs.0c06779
J. Am. Chem. Soc. 2020, 142, 15438−15444